A hybrid multi-modal visual data cross fusion network for indoor and outdoor segmentation

Sijie Hu, Fabien Bonardi, Samia Bouchafa, Désiré Sidibé

A hybrid multi-modal visual data cross fusion network for indoor and outdoor segmentation

Sijie Hu*†, Fabien Bonardi*, Samia bouchafa* and Désiré Sidibé*

*Université Paris-Saclay, Univ Evry, IBISC, 91020, Evry-Courcouronnes, France

† Email: sijie.hu@universite-paris-saclay.fr

Abstract—**Multi-modal scene parsing is a prevalent topic in robotics and autonomous driving since the knowledge of different modalities can complement each other. Recently, the success of self-attention-based methods has demonstrated the effectiveness of capturing long-range dependencies. However, the tremendous cost dramatically limits the application of this idea in multi-modal fusion. To alleviate this problem, this paper designs a multi-modal cross-fusion block (AC) and its elegant variant (EAC) based on an additive attention mechanism to capture global awareness among different modalities efficiently. Moreover, a simple yet efficient transformer-based trans-context block (TC) is also presented to connect the contextual information. Based on the above components, we propose light HCFNet, which can explore long-range dependencies of multi-modal information while keeping local details. Finally, we conduct comprehensive experiments and analyses on both indoor (NYUv2-13, -40) and outdoor (Cityscapes-11) datasets. Experiment results show that the proposed HCFNet achieved 66.9% and 51.5% mIoU on NYUv2-13 and -40 classes settings, which outperform current start-of-the-art multi-model methods. Our model also shows a competitive mIoU of 80.6% on the Cityscapes-11 dataset. The code will be available at https://github.com/Superjie13/HCFNet.**

I. INTRODUCTION

As a fundamental task, semantic segmentation has received a broad range of attention in the computer vision community and industry. Depth information as an auxiliary provides shape and geometry cues of the surroundings that complement the RGB data, thus introducing depth information to improve the model's performance has become a trend in robotics and autonomous driving. To this end, a series of networks with RGB-D as input appeared. These methods directly concatenate RGB and Depth images [1]–[3] or treat them in two branches [4]–[7].

Recently, self-attention-based transformer architecture has attracted attention in the computer vision community due to its flexibility in long-range modeling dependencies and its remarkable success in natural language processing (NLP). Therefore, well-designed transformer block (TB) or their variants are introduced to replace the region-wise convolution structure [8], [9], and their results have shown that a global view brought by self-attention helps draw a better performance. However, the tremendous computation severely restricts its application in computer vision, especially on some resource-limited and low-latency systems. To alleviate this shortcoming, some works were designed to process images at a low resolution [8], [10] or using a sliding window [9], [11]; others borrowed the idea from CNN-like architecture

and introduce pyramid structure [12], [13]. Although various solutions for building long-range dependencies of individual RGB image reasoning emerged, the exploration of fusing RGB and Depth data for scene parsing is very limited. Existing multi-modal methods mainly deploy TB in a hybrid structure, i.e., mixing CNN and transformer, to ingest the advancement of both convolution and TB. The mainstream combinations of CNN and TB operations are (1) cascade: convolution operations are used to process high-resolution data and then followed by TBs to process low-resolution data. (2) parallel: CNNs are used as the backbone network for feature extraction, while TBs are independent modules to address the data fusion and exchange between different modalities. For example, [14] introduces the TB into the last two layers of the encoder in U-Net [15], reducing the calculation amount. [16] treat TB as an independent part and stack multiple self-attention modules to incorporate the global attention of the 3D scene. Compared with parallel structure, cascade structure fails to capture a larger context at the shallow level, and all existing methods rudely use the TB, so they inevitably bear the burden of the TB, i.e., the tremendous calculation.

We argue that the global attention founded by TB is the crucial reason for the success of Transformer. Recently, [17] proposed an efficient Transformer variant based on additive attention to achieve global attention modeling in linear complexity. Inspired by this, we propose a well-designed additive-attention-based cross-fusion block (AC) to incorporate depth information into RGB and form long-range dependencies between depth and RGB features. Besides, we present EAC block, an efficient variant of AC, which efficiently builds global contexts while maintaining fine-grained shape details. On the other hand, we offer a simple yet efficient trans-context module (TC) to enrich contextual information and capture a global context from fused features. Based on the above modules, we design a hybrid cross fusion network (HCFNet), as shown in Figure 1. With all the ideas, our method benefits from building global awareness while significantly reducing computational consumption. The formed global awareness crosses RGB and depth, bringing integrated information from different modalities. We report the experimental results on two commonly used datasets, namely NYUv2(-13, -40) [18] and Cityscapes-11 [19], to verify the effectiveness of the proposed method in both indoor and outdoor scenarios.

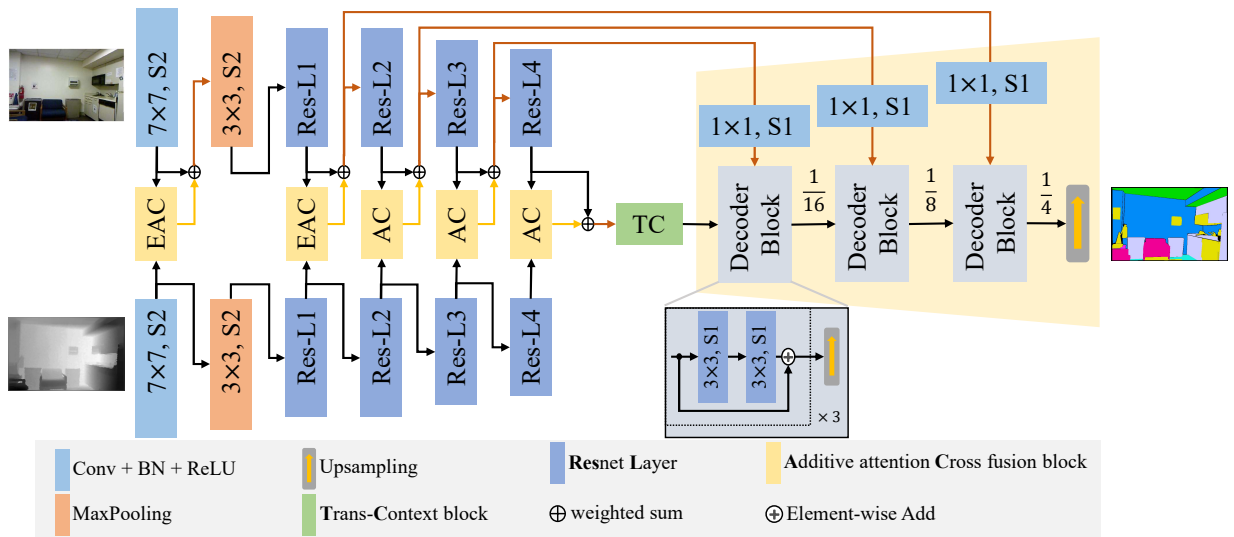The main contributions of this paper are summarized as follows:

Fig. 1. Structure of HCFNet. This network takes two inputs, i.e., RGB and Depth. $7 \times 7, S2$ means convolution with kernel size 7 and stride 2, and BN denotes batch normalization.

- We propose an efficient hybrid RGB-D data fusion network called HCFNet for semantic segmentation.
- We propose a light data fusion block named additive attention cross fusion block (AC), and its variant (EAC), to form long-range dependencies cross depth and RGB features. Moreover, we offer a simple yet efficient trans-context module (TC) based on TB to build a global view of fused features.
- We experimentally validate the proposed HCFNet on indoor and outdoor datasets, including NYUv2(-13, -40) and Cityscapes-11. Results show that our method achieves 66.9% mIoU on NYUv2-13, 51.5% mIoU on NYUv2-40, and 80.6% mIoU on Cityscapes-11 dataset, which is quite competitive compared with state-of-the-art RGB-D fusion methods.

II. RELATED WORK

A. Global attention and Transformer

Transformer was firstly proposed by [20] for NLP tasks. The core component is built upon multi-head self-attention, which can model the long-range dependencies within a sequence. A similar idea was introduced by [21] in computer vision to design a non-local block to build the global relationship between pixels. [22] proposed a full attention block based on a non-local block that computes global attention along both channel and spatial dimensions. As a pioneer of visual Transformer, [10] used pure Transformer structure to classify images and achieved promising results. [8] extended the work in [10] to semantic segmentation. Then, [9], [11] calculate self-attention in sub-windows to alleviate the resolution disaster, and apply Transformer structure to dense segmentation. [12], [13], [23] employed a pyramid or hierarchical Transformer structure to improve the computational efficiency of the model for segmentation. Moreover, [24] proposed a 'transposed' self-attention

that computes global attention across feature channels so that the computational complexity is linear. Recently, [17] offered a variant of Transformer, in which additive attention replaces self-attention to establish global awareness. Compared with other global attention mechanisms, the calculation of additive attention is more efficient, so this article establishes a more general cross-modal fusion attention mechanism based on additive attention.

B. RGB-D semantic segmentation

With a more affordable depth sensor, semantic segmentation leveraged by the complementary geometric information of depth has drawn attention. However, the large noise in depth and the asymmetry between RGB and depth data make it challenging to integrate RGB and depth features effectively. In general, existing semantic segmentation structures include two stages: encoding and decoding. Concretely, input data are first encoded to form contextual feature embeddings then decoded to recover semantic information [25]. Some work [3], [26], [27] redesigned the convolution operation based on the characteristics of RGD-D data. [28] presented depth-aware operations to leverage depth similarity between pixels. [3] proposed a shape-aware convolutional layer. This convolutional layer is composed of two independent learnable components in the learning phase, and all the learnable parameters in the inference phase can be re-weight into a standard convolution operation. [26] introduced malleable 2.5D convolution to learn the receptive field along the depth axis. In contrast, most approaches are proposed to feed RGB and depth to two parallel branches [4], [5], [7], [29], [30]. For example, [31] employed two separate encoder-decoders to process RGB and depth, respectively, during which the manually designed gated fusion layer is used to fuse information from different streams. [32] used skip-connection to transmit the encoded multi-modal information to the decoder. [5]–[7] fuse the features
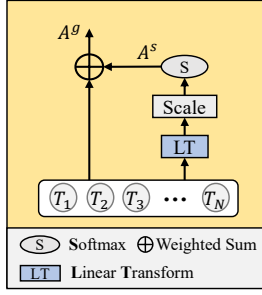
Fig. 2. Structure of the additive attention block

at different stages of the encoding process. Recently, [30] applied a shallow encoder and factorized convolutions to create a lightweight model for real-time operations.

Unlike the above methods, we design a hybrid cross fusion network that takes advantage of long-range dependencies in the Transformer while maintaining the model's efficiency.

III. METHOD

A. Overview of the method

An overview of our hybrid cross fusion network (HCFNet) is presented in Figure 1. The structure is derived from a general and classical multi-modal semantic segmentation paradigm, i.e., two encoders for extracting features from RGB and Depth and one decoder for reconstructing features from embeddings. Similar to [5], [30], we use independent modules to achieve data fusion of different modalities and pass features to the decoder via skip-connections. The decoder is divided into multiple stages. In each stage, feature maps are first treated by a series of residual blocks [33] and then upsampled by a factor of 2. The final output of the decoder is upsampled by the factor of 4 to recover the original resolution. Our network uses shallow encoders (i.e., ResNet-34 [33]) as the backbone for feature extraction of both RGB and Depth streams to reduce the footprint at runtime. In addition, we introduce additive attention cross fusion blocks (AC) and EAC to fuse valuable information efficiently during encoding and trans-context block (TC) to enrich contextual features at the end of the encoder.

B. AC block and its variant EAC

1) Additive attention: Additive attention was first introduced in [17], which brings an effective global attention mechanism to recalibrate the features within a sequence. A basic form of additive attention is depicted in Figure 2. We first summarize each token (T_i, $i \in [1 \dots N]$) into an attention scores by a linear transformation and a scale factor of $\sqrt{d}$, where d is the number of channels in a token. Then each obtained attention score is normalized by a softmax operation to get A_i^s. The process can be formulated as:

$$A_i^s = \frac{\exp(\mathbf{W_a}^T T_i / \sqrt{d})}{\sum_{j=1}^{N} \exp(\mathbf{W_a}^T T_j / \sqrt{d})}, \tag{1}$$
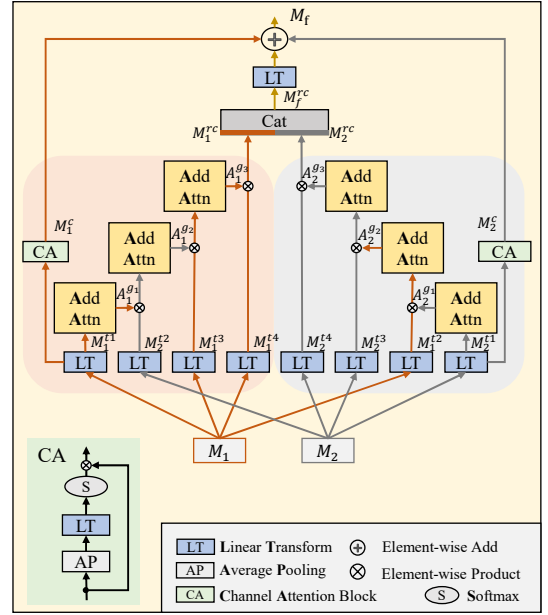

Fig. 3. Structure of the proposed AC block in Figure. Add-Attn is the additive attention shown in Figure 2

where N refers to the number of tokens and $i \in [1 \dots N]$, $\mathbf{W_a} \in \mathbb{R}^d$ is learnable weights of linear transformation. The final global attention is obtained by weighted sum:

$$A^g = f(T) = \sum_{i=1}^{N} A_i^s \cdot T_i. \tag{2}$$

Note that additive attention has multiple heads as in the standard self-attention.

2) AC block: As shown in Figure 3, the **A**dditive attention **C**ross fusion block (AC) adopts a symmetrical structure. $M_i \in \mathbb{R}^{d \times N}$, $i \in [1, 2]$ denote the inputs from two encoders. Concretely, M_1 and M_2 are first processed by four linear transformation (LT) units, respectively:

$$M_i^{t_j} = \mathbf{W_i^j}^T M_i, \tag{3}$$

where $\mathbf{W_i^j} \in \mathbb{R}^{d \times d}$ refers to learnable parameters in LT, $i \in [1, 2]$, $j \in [1, 2, 3, 4]$. For the left part, M_1^{t1} is fed into additive attention blocks to get a global attention score $A_1^{g1} \in \mathbb{R}^d$ and then element-wise multiplied by M_2^{t2} to integrate attention score of M_1 to the feature map of M_2. Then, in the same way, we build attention scores A_1^{g2}, and A_1^{g3} while only considering the feature map of M_1. For the right part, we use the same way to get A_2^{g3}. Meantime, we also introduce the information from M_1 as an additional reference. Note that we use the knowledge from another modality to calibrate the long-range dependencies building process in the current modality. This strategy makes it easier for AC block to establish cross attention from one modality to another. This process can be formalized as:

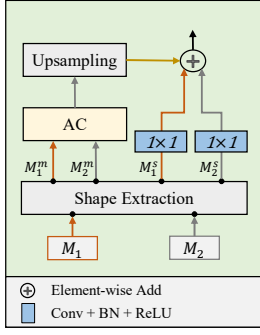$$A_i^{g3} = f\Big(f\big(f(M_i^{t_1}) \otimes M_{3-i}^{t_2}\big) \otimes M_i^{t_3}\Big), \tag{4}$$

Fig. 4. Structure of the proposed EAC block

Fig. 5. An example of Shape extraction in Figure 4

where $i \in [1, 2]$, f denotes additive attention operation (see equation 2) and $\otimes$ denotes element-wise multiplication operation.

At the same time, M_1^{t1} and M_2^{t1} are respectively transferred into two bypass branch modules to get M_1^c and M_2^c. The bypass branch module is designed similar to the classical channel attention (CA) mechanism, which can be described as:

$$
\begin{aligned}
M_i^c &= \mathbf{Softmax}(M_i^t) \otimes M_i^{t1} \\
M_i^t &= \mathbf{W_i^c}^T M_i^a \\
M_i^a &= \mathbf{AvePooling}(M_i^{t1}),
\end{aligned}
\tag{5}
$$

where $i \in [1, 2]$, $\mathbf{W_i^c} \in \mathbb{R}^{d \times d}$ are the parameters of LT, $\mathbf{AvePooling}$ is average pooling operation along tokens.

Next, the generated A_1^{g3} and A_2^{g3} are respectively element-wise multiplied by M_1^{t4} and M_2^{t4}, and then concatenated along channel axis to get M_f^{rc}. Finally, after a linear transformation, M_f^{rc} is element-wise added with M_1^c and M_2^c to get the final output M_f:

$$
\begin{aligned}
M_f &= M_1^c + M_2^c + M_t^{rc} \\
M_t^{rc} &= \mathbf{W^{rc}}^T M_f^{rc},
\end{aligned}
\tag{6}
$$

where $\mathbf{W^{rc}} \in \mathbb{R}^{2d \times d}$ are parameters of LT and $+$ refers to element-wise addition operation.

The idea behind this design is very intuitive. We use the global attention from M_1 to calibrate the features in M_2. Then the calibrated feature map of M_2 regenerates new global attention, which is further used to re-calibrate the features in M_1, and vice versa. Therefore, the block fully evaluates the interrelationship between different modalities to achieve a better efficient fusion. Note that AC block can also perform cross-feature fusion in sub-windows for more flexible analysis of local features.

3) EAC block: **E**fficient **A**dditive attention **C**ross fusion block (EAC) is a variant of AC (section III-B2), designed to puzzle out the excessive consumption of building long-range dependencies under large resolution input. We consider that establishing global context information under full-resolution input will introduce redundancy, which leads to unnecessary
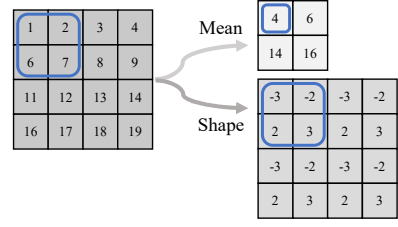
TABLE I
CONFIGURATION OF AC OR EAC BLOCKS IN FIGURE 1

block	(c1, c2)	im_scale	sw	sub_w	heads
EAC	(64, 64)	1/2	(8, 8)	(2, 2)	8
EAC	(64, 64)	1/4	(4, 4)	(2, 2)	8
AC	(128, 128)	1/8	-	(4, 4)	16
AC	(256, 256)	1/16	-	(h/16, w/16)	32
AC	(512, 512)	1/32	-	(h/32, w/32)	64

h and w refer to the height and width of original resolution, c_1 and c_2 denote channels of each modality, im_scale denotes the ratio of the current input size to the original image size, sw denotes the size of sliding window in EAC block, sub_w denotes the size of sub-windows in AC block, and $heads$ denotes the number of head in additive attention.

calculations. In addition, fine-grained shape information is essential for establishing target contours. Accordingly, we decouple the process of establishing global context information and contour information. To do so, we design a shape extraction module in EAC block. An example for demonstrating the shape extraction module is shown in Figure 5. For each input, briefly, we compute the mean value of each local area by a sliding window with a certain stride which is equal to the size of the sliding window, to obtain the mean map. Then, the mean value in each local window is removed to obtain the shape map. Thanks to the parallel computing of Pytorch [34], this process can be implemented very efficiently.

EAC block is shown in Figure 4, we first build the mean map M^m and the shape map M^s of the input M_1 and M_2 through a shape extraction module. The extracted mean information M_1^m and M_2^m are input to the AC block to get the global context attention, and then followed by an upsampling operation to recover the resolution. The extracted shape information is processed by a pixel-wise convolution. Finally, mean information and shape information are integrated by element-wise addition. Table I shows the configuration of AC or EAC blocks at every encoding stage.
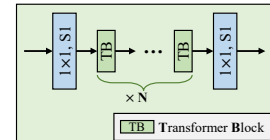

Fig. 6. Structure of the proposed TC block in Figure 1

Model	BackBone	mIoU (%)		FPS
		NYUv2-13	NYUv2-40	
FuseNet [29]	Vgg-16	54.6	-	15.1
RedNet [5]	ResNet-50	64.0	-	24.2
ACNet [7]	ResNet-50	64.8	48.3*	17.9
ESANet† [30]	ResNet-34	65.1	50.3*	39.7
ESANet [30]	ResNet-50	65.9	50.5*	44.6
ShapeConv [3]	ResNext-101	65.1*	51.3*◇	12.3
HCFNet(Ours)	ResNet-34	65.8	49.9	36.2
HCFNet†(Ours)	ResNet-34	66.7	50.7	31.7
HCFNet(Ours)	ResNet-50	66.9	51.5	22.5

∗ denotes that we report the result from the original paper, † denotes that the BasicBlock is replaced by NBt1D [35], and ◇ refers to multi-scale testing strategy.

TABLE III
PERFORMANCE OF DIFFERENT METHODS ON CITYSCAPES-11 VAL SET.

Model	BackBone	mIoU (%)	FPS	Latency
RedNet [5]	ResNet-50	79.6	26.1	0.038
ACNet [7]	ResNet-50	80.0	19.6	0.051
ESANet [30]	ResNet-34	77.8	47.6	0.021
ESANet† [30]	ResNet-34	78.5	42.1	0.024
HCFNet (Ours)	ResNet-34	78.4	39.0	0.025
HCFNet† (Ours)	ResNet-34	78.9	35.2	0.028
HCFNet (Ours)	ResNet-50	80.6	25.3	0.039

∗ denotes that we report the result from the original paper and † denotes that the BasicBlock is replaced by NBt1D [35].

C. TC block

As shown in Figure 6, the **T**rans-**C**ontext block is composed of convolution and transformer blocks. Specifically, we first project the input channels through a 1×1 convolution, and then several TBs are applied to obtain complex context. Finally, we restore the number of input channels through another 1×1 convolution. The whole process is straightforward but very convenient. Note that the TB in our TC block can utilize existing well-designed methods, such as [10], [11]. We reimplement and employ TB of [17] in our TC block.

IV. EXPERIMENTS

A. Datasets and Implementation Details

1) NYUv2: NYUv2 is a popular dataset for indoor scene analysis. It contains 1449 indoor finely annotated RGB-D images, in which 795 are used for training and 654 for testing. All images are provided with a resolution of 640×480. We follow [3] using the train/test splits as provided by the dataset and report results on the 13 and 40 classes [18] settings.

2) Cityscapes: The Cityscapes dataset is a large-scale database for urban street scene parsing. It contains 5000 finely annotated images captured from 50 cities with 19 semantic object categories, in which 2875 images are used for training, 500 images and 1525 images are used for validation and testing separately. All images are provided with a resolution of 2048×1024. We report results on the reduced 11 classes [4] setting.

3) Implementation Details: We implement our network based on Pytorch [34], and all experiments are run on a Nvidia RTX3090 GPU with 24GB memory. For the network, we take Resnet-34 initialized with the pre-trained weight on ImageNet [36] as the backbone of both encoders. We train our model for 500 epochs with a mini-batch size of 8 for the NYUv2 dataset and 300 epochs with a mini-batch size of 16 for the Cityscapes dataset. As for optimization, NYUv2 dataset is trained on SGD optimizer with a initial learning rate of 0.015 and Cityscapes dataset is trained on Adam optimizer with an initial learning of 0.0001. Following [30], we employ a one-cycle learning

rate policy. Moreover, we set the number of TB in TC block (N) as 3. The image input size is set to 640×480 on the NYUv2 dataset and 768×384 on the Cityscapes dataset. If not otherwise noted, the inputs of all models are RGB and depth images. Note that before training on the Cityscapes dataset, we follow the official guide to generate a depth map from the original disparity data [19]. Random scaling, cropping, and flipping are applied for data augmentation to increase the number of training samples further. We evaluate our model based on mean intersection over union (mIoU). In addition, we still care for the frame per second (FPS) rate because of the computational burden.

B. Comparative results

1) Results on NYUv2: Table II compares the performance of our proposed methods with start-of-the-art methods. For a comprehensive comparison, we re-implement the prevalent multi-modal fusion methods based on their official repository and report the results on NYUv2-13 setting. Besides, we report our results on the commonly used NYUv2-40 setting. For the methods tested in the original paper, we use the reported results directly. We then follow [30] to modify our model by replacing BasicBlock with Non-Bottleneck-1D-Block (NBt1D) [35]. In our experiments, we also pay attention to FPS since they reflect the actual operating efficiency of the model. All FPS are executed at the input resolution of 640×480 on a laptop with Intel i7-9750 CPU and Nvidia RTX 2080 8G GPU. We noticed that the model based on NBt1D runs slower than the original model, which is inconsistent with the report in [30]. We consider this is because the 3×3 convolution is fully optimized in the computer environment. In table II we can see that our model outperforms current state-of-the-art methods on both NYUv2-13 and -40 classes settings while keeping a fast inference time. In addition, we found that our method is capable of capturing overall contextual information while extracting valuable details. Please refer to the supplementary material for some qualitative results.

2) Results on Cityscapes: To exhibit the capabilities of our model in outdoor scenarios, we evaluate our model on the Cityscapes-11 dataset. Specifically, we resize the input image to a resolution of 768×384. All models are trained and evaluated at the same resolution. Note that all models are

configured to the same training strategy, unless a different setting is provided in the original implementation. We observed that the Cityscapes dataset is very sensitive to the backbone, and a well pre-trained backbone can significantly improve the performance. As shown in Table III, our model yielded a very comparable result when using ResNet34 as backbone, and improved the segmentation results when using ResNet50 as backbone.

C. Ablation Analysis

To verify the functionality of the components of our model, we conduct an ablation study on the NYUv2-13 dataset. We use the network architecture in Figure 1 as the basic structure. For a fair comparison, network architecture and hyper-parameters in different experiments are fixed. In ablations, we first evaluate the influence of different fusion methods, namely Add, ACM, SE, which have been used in recent start-of-the-art models. Specifically, Add [5], [29] simply adds the data of different modalities directly. ACM [7] and SE [30] calculate each modality's attention through the Attention Complementary module (ACM) and Squeeze-and-Excitation module (SE) before fusion. Then we estimate the impact of the TC block on performance. Table IV summarizes the results of this ablation study on HCFNet.

From Experiment 1 to Experiment 3, we use different fusion methods to replace AC and EAC blocks of the original HCFNet while removing the TC block. As we can see, the proposed AC method is superior to other fusion methods by a large margin. Figure 7 visualized the feature maps of the output of different fusion methods at different stages in HCFNet. Specifically, in B1 and B2, we use the EAC blocks. We can see that EAC can remove redundant facts in the scene without losing valuable information. In B3-B5, AC blocks are deployed. It can be seen that the targets of interest are effectively activated, and it has a more extensive range and more accurate position than other fusion methods. This further verifies that the global awareness obtained in the AC module helps the model understand the scene. Please refer to the supplementary material for additional analysis of the AC/EAC block.

In addition, after deploying the TC block, the performance of our model is significantly improved (+0.6%), which reveals that it is practical to further establish long-range dependencies in the fused features. In the final experiment, we replaced the EAC block in Table I with the AC block, which caused a decrease in model performance. This echoes our previous argument that the context contains much redundant information under large-resolution input, which will lead to unnecessary calculations and confusion. In contrast, our proposed AC block can efficiently establish long-range awareness, and with the help of the EAC block, redundant information can be eliminated without destroying local details while significantly reducing the amount of calculation. Finally, the proposed TC block can further coordinate information fusion and establish a more significant receptive field.

	Model	Fusion	Context	mIoU (%)
1		Add [5]	None	63.3
2		ACM [7]	None	64.1
3	HCFNet	SE [30]	None	63.9
4		AC* (Ours)	None	65.2
5		AC* (Ours)	TC	65.8
6		AC (Ours)	TC	65.1

$\star$ denotes we follow Table I to configure AC and EAC blocks.
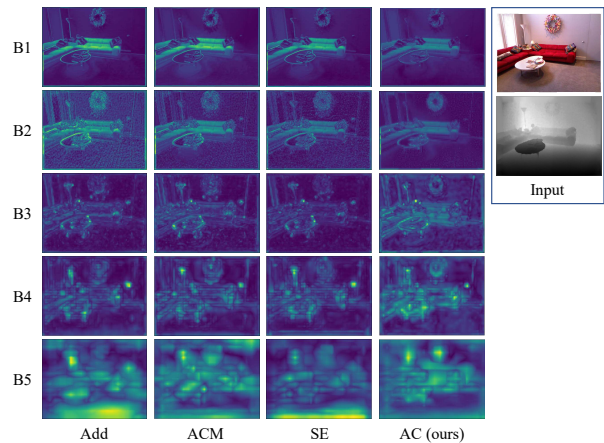

Fig. 7. Visualization of feature maps of different fusion methods. B1-B5 refers to the output of different fusion blocks in the encoding part of Figure 1. Note that the sample comes from the NYUv2 test set, and all outputs are resized to a resolution of 640×480 for a best of view.

V. CONCLUSION

In this paper, we designed a novel multi-modal visual data fusion method, which can efficiently integrate data from different modalities. It also ensures that the model retains valuable local details after fusion while having a global receptive field. Precisely, we customized a multi-modal fusion block named AC block based on the additive attention mechanism, which assists form global awareness inter- and inner-modalities. Then, we proposed the EAC block, an efficient variant of the AC block, to efficiently build global attention and keep details under high-resolution input. On the other hand, based on the transformer block, we offered a simple yet effective context fusion block called trans-context (TC) block for further connecting the context output from the encoder. Together with the proposed well-designed components, we present HCFNet for semantic segmentation of indoor and outdoor scenarios. Finally, comprehensive experiments and ablation studies verified the effectiveness of our network and different components.

In the future, we will further optimize the structure of the model and exploit the possibilities of our model on different other modalities such as infrared or polarimetry.

REFERENCES

[1] C. Couprie, C. Farabet, L. Najman, and Y. LeCun, "Indoor semantic segmentation using depth information," arXiv preprint arXiv:1301.3572, 2013.

[2] H. Xu, J. Ma, J. Jiang, X. Guo, and H. Ling, "U2fusion: A unified unsupervised image fusion network," IEEE Transactions on Pattern Analysis and Machine Intelligence, 2020.

[3] J. Cao, H. Leng, D. Lischinski, D. Cohen-Or, C. Tu, and Y. Li, "Shapeconv: Shape-aware convolutional layer for indoor rgb-d semantic segmentation," in Proceedings of the IEEE/CVF International Conference on Computer Vision, 2021, pp. 7088–7097.

[4] A. Valada, R. Mohan, and W. Burgard, "Self-supervised model adaptation for multimodal semantic segmentation," International Journal of Computer Vision, vol. 128, no. 5, pp. 1239–1285, 2020.

[5] J. Jiang, L. Zheng, F. Luo, and Z. Zhang, "Rednet: Residual encoder-decoder network for indoor rgb-d semantic segmentation," arXiv preprint arXiv:1806.01054, 2018.

[6] X. Chen, K.-Y. Lin, J. Wang, W. Wu, C. Qian, H. Li, and G. Zeng, "Bi-directional cross-modality feature propagation with separation-and-aggregation gate for rgb-d semantic segmentation," in Computer Vision–ECCV 2020: 16th European Conference, Glasgow, UK, August 23–28, 2020, Proceedings, Part XI 16. Springer, 2020, pp. 561–577.

[7] X. Hu, K. Yang, L. Fei, and K. Wang, "Acnet: Attention based network to exploit complementary features for rgbd semantic segmentation," in 2019 IEEE International Conference on Image Processing (ICIP). IEEE, 2019, pp. 1440–1444.

[8] R. Strudel, R. Garcia, I. Laptev, and C. Schmid, "Segmenter: Transformer for semantic segmentation," arXiv preprint arXiv:2105.05633, 2021.

[9] Z. Liu, Y. Lin, Y. Cao, H. Hu, Y. Wei, Z. Zhang, S. Lin, and B. Guo, "Swin transformer: Hierarchical vision transformer using shifted windows," arXiv preprint arXiv:2103.14030, 2021.

[10] A. Dosovitskiy, L. Beyer, A. Kolesnikov, D. Weissenborn, X. Zhai, T. Unterthiner, M. Dehghani, M. Minderer, G. Heigold, S. Gelly et al., "An image is worth 16x16 words: Transformers for image recognition at scale," arXiv preprint arXiv:2010.11929, 2020.

[11] X. Chu, Z. Tian, Y. Wang, B. Zhang, H. Ren, X. Wei, H. Xia, and C. Shen, "Twins: Revisiting the design of spatial attention in vision transformers," in Thirty-Fifth Conference on Neural Information Processing Systems, 2021.

[12] W. Wang, E. Xie, X. Li, D.-P. Fan, K. Song, D. Liang, T. Lu, P. Luo, and L. Shao, "Pyramid vision transformer: A versatile backbone for dense prediction without convolutions," arXiv preprint arXiv:2102.12122, 2021.

[13] ——, "Pvtv2: Improved baselines with pyramid vision transformer," arXiv preprint arXiv:2106.13797, 2021.

[14] Q. Jia and H. Shu, "Bitr-unet: a cnn-transformer combined network for mri brain tumor segmentation," arXiv preprint arXiv:2109.12271, 2021.

[15] O. Ronneberger, P. Fischer, and T. Brox, "U-net: Convolutional networks for biomedical image segmentation," in International Conference on Medical image computing and computer-assisted intervention. Springer, 2015, pp. 234–241.

[16] A. Prakash, K. Chitta, and A. Geiger, "Multi-modal fusion transformer for end-to-end autonomous driving," in Proceedings of the IEEE/CVF Conference on Computer Vision and Pattern Recognition, 2021, pp. 7077–7087.

[17] C. Wu, F. Wu, T. Qi, Y. Huang, and X. Xie, "Fastformer: Additive attention can be all you need," arXiv preprint arXiv:2108.09084, 2021.

[18] N. Silberman, D. Hoiem, P. Kohli, and R. Fergus, "Indoor segmentation and support inference from rgbd images," in European conference on computer vision. Springer, 2012, pp. 746–760.

[19] M. Cordts, M. Omran, S. Ramos, T. Rehfeld, M. Enzweiler, R. Benenson, U. Franke, S. Roth, and B. Schiele, "The cityscapes dataset for semantic urban scene understanding," in Proceedings of the IEEE conference on computer vision and pattern recognition, 2016, pp. 3213–3223.

[20] A. Vaswani, N. Shazeer, N. Parmar, J. Uszkoreit, L. Jones, A. N. Gomez, Ł. Kaiser, and I. Polosukhin, "Attention is all you need," in Advances in neural information processing systems, 2017, pp. 5998–6008.

[21] X. Wang, R. Girshick, A. Gupta, and K. He, "Non-local neural networks," in Proceedings of the IEEE conference on computer vision and pattern recognition, 2018, pp. 7794–7803.

[22] Q. Song, J. Li, C. Li, H. Guo, and R. Huang, "Fully attentional network for semantic segmentation," arXiv preprint arXiv:2112.04108, 2021.

[23] E. Xie, W. Wang, Z. Yu, A. Anandkumar, J. M. Alvarez, and P. Luo, "Segformer: Simple and efficient design for semantic segmentation with transformers," arXiv preprint arXiv:2105.15203, 2021.

[24] A. El-Nouby, H. Touvron, M. Caron, P. Bojanowski, M. Douze, A. Joulin, I. Laptev, N. Neverova, G. Synnaeve, J. Verbeek et al., "Xcit: Cross-covariance image transformers," arXiv preprint arXiv:2106.09681, 2021.

[25] Y. Zhang, D. Sidibé, O. Morel, and F. Mériaudeau, "Deep multimodal fusion for semantic image segmentation: A survey," Image Vis. Comput., vol. 105, p. 104042, 2021. [Online]. Available: https://doi.org/10.1016/j.imavis.2020.104042

[26] Y. Xing, J. Wang, and G. Zeng, "Malleable 2.5 d convolution: Learning receptive fields along the depth-axis for rgb-d scene parsing," in Computer Vision–ECCV 2020: 16th European Conference, Glasgow, UK, August 23–28, 2020, Proceedings, Part XIX 16. Springer, 2020, pp. 555–571.

[27] L.-Z. Chen, Z. Lin, Z. Wang, Y.-L. Yang, and M.-M. Cheng, "Spatial information guided convolution for real-time rgbd semantic segmentation," IEEE Transactions on Image Processing, vol. 30, pp. 2313–2324, 2021.

[28] W. Wang and U. Neumann, "Depth-aware cnn for rgb-d segmentation," in Proceedings of the European Conference on Computer Vision (ECCV), 2018, pp. 135–150.

[29] C. Hazirbas, L. Ma, C. Domokos, and D. Cremers, "Fusenet: Incorporating depth into semantic segmentation via fusion-based cnn architecture," in Asian conference on computer vision. Springer, 2016, pp. 213–228.

[30] D. Seichter, M. Köhler, B. Lewandowski, T. Wengefeld, and H.-M. Gross, "Efficient rgb-d semantic segmentation for indoor scene analysis," in 2021 IEEE International Conference on Robotics and Automation (ICRA). IEEE, 2021, pp. 13 525–13 531.

[31] Y. Cheng, R. Cai, Z. Li, X. Zhao, and K. Huang, "Locality-sensitive deconvolution networks with gated fusion for rgb-d indoor semantic segmentation," in Proceedings of the IEEE conference on computer vision and pattern recognition, 2017, pp. 3029–3037.

[32] F. Fooladgar and S. Kasaei, "Multi-modal attention-based fusion model for semantic segmentation of rgb-depth images," arXiv preprint arXiv:1912.11691, 2019.

[33] K. He, X. Zhang, S. Ren, and J. Sun, "Deep residual learning for image recognition," in Proceedings of the IEEE conference on computer vision and pattern recognition, 2016, pp. 770–778.

[34] A. Paszke, S. Gross, F. Massa, A. Lerer, J. Bradbury, G. Chanan, T. Killeen, Z. Lin, N. Gimelshein, L. Antiga et al., "Pytorch: An imperative style, high-performance deep learning library," arXiv preprint arXiv:1912.01703, 2019.

[35] E. Romera Carmena, J. M. Álvarez López, L. M. Bergasa Pascual, R. Arroyo Contera et al., "Erfnet: efficient residual factorized convnet for real-time semantic segmentation," 2018.

[36] O. Russakovsky, J. Deng, H. Su, J. Krause, S. Satheesh, S. Ma, Z. Huang, A. Karpathy, A. Khosla, M. Bernstein et al., "Imagenet large scale visual recognition challenge," International journal of computer vision, vol. 115, no. 3, pp. 211–252, 2015.